TEMPERATURE DEPENDENCE OF MATERIAL PROPERTIES AND ITS INFLUENCE ON THE THERMAL DISTRIBUTION IN REGENERATIVELY COOLED COMBUSTION CHAMBER WALLS

M. Oschwald, D. Suslov, A. Woschnak
German Aerospace Center, Institute for Space Propulsion, Lampoldshausen, D-74239 Hardthausen

Introduction

Combustion chamber wall structures regeneratively cooled with liquid hydrogen experience a wide range of temperatures during a firing cycle. Before ignition liquid hydrogen with a temperature of about 35K enters the cooling channels and cools down the wall structures accordingly. After ignition the hot gas side wall temperature increases to about 800K. On the coolant side wall temperatures vary dependent on design and position typically between less than 100K and more than 600K. Properties of materials used for the manufacturing of combustion chambers exhibit in this wide temperature range a marked temperature dependence. Especially in the low temperature limit the thermal conductivity λ, the specific heat c_V, and the thermal expansion coefficient α show strong variations.

Life predictions for combustion chambers rely on the modelling of transient thermal fields and thermal gradients in the structure during an operational cycle [1]. A typical value for the sensitivity is a life time reduction of 50% for an increase of the hot gas side wall temperature by 40K [2].

The question therefore arises whether the temperature dependence of the thermo-physical and mechanical material properties have to be taken into account during the thermal design of cooling channels of regeneratively cooled combustion chambers. During stationary thermal conditions only the thermal conductivity controls the thermal field. During start-up and shut-down transients also the specific heat comes into play. A temperature dependence of these properties may influence the thermal field in the structure and the associated thermal loads. A temperature dependence of the expansion coefficient is important for the analysis of thermal stress, relevant for the life prediction of components.

The paper starts with a general discussion of the behaviour of the thermal conductivity λ, the specific heat c_V, and the thermal expansion coefficient α at low temperatures. In the focus of the analysis is the consequence of the variation of λ and c_V with temperature on the sta-

tionary and transient thermal field in the wall of the L42 combustor, a liquid hydrogen cooled model combustor operated at DLR Lampoldshausen. This model combustor has been used in extensive test campaigns for the determination of heat transfer properties at representative conditions [3, 7].

For the CuCrZr-alloy used as chamber material the variation of the thermal conductivity with temperature has been determined experimentally. The role of this temperature dependence for the thermal field in the wall structure is evaluated for the cooling channel geometries used in the L42-combustor.

Finally the temperature dependence of the specific heat and its influence on the thermal gradients is discussed.

Low Temperature Behavior of Material Properties

Specific Heat

The temperature dependence of the specific heat at low temperatures is a standard example for material behaviour that can be only explained with quantum mechanics [4,5].

The specific heat of solids at high temperatures approaches a constant value c_V=3Nk$_B$ =24.94 J/mol/K (N is the number of atoms, k$_B$ the Boltzmann-constant). At sufficiently high temperatures all possible lattice vibrations are excited. At low temperature the thermal energy becomes to small to excite modes with high excitation energy. The number of degrees of freedom participating at the energy transfer is reduced, c_V is decreasing. In the frame of the Debey-model [5] this behaviour is described correctly. The temperature dependence is controlled by the material specific Debye-temperature Θ_D. Especially the Debey model is in agreement with the experimentally found behaviour for the limit $T<<\Theta_D$, which is $c_V \propto (T/\Theta_D)^3$. Approaching absolute zero, the specific heat disappears.

In fig. 1 the specific heat calculated according to the Debey-model and the data from a database for low temperature properties are shown. At 77K the specific heat has dropped to about 50% of the value in the $T>>\Theta_D$ limit, at the boiling temperature of LH2 c_V has about 3% of this value. The specific heat of Cu therefore varies significantly in the temperature range of interest.

The value of the specific heat is not sensitive to minor additions of foreign elements.

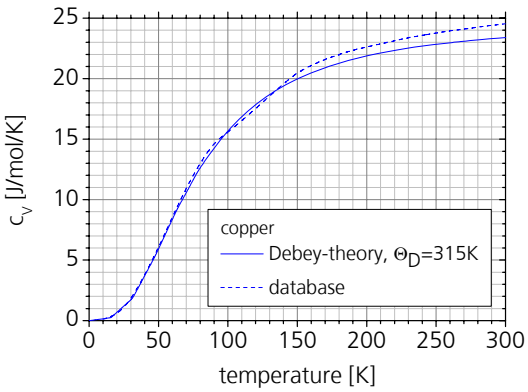

Fig. 1

Thermal Conductivity

Heat transport in a solid is based on two transport mechanisms: anharmonicities of the interaction potentials result in a coupling of different vibrational states (phonons) of the lattice and free conducting electrons contribute to the transport of thermal energy in the solid. In pure metals the contribution of the electrons is significantly larger than that of phonon transport at all temperatures. In metals with impurities or alloys the phonons are scattered at lattice defects and foreign atoms and both contributions can become of comparable size.

Thermal conductivities λ for pure copper and an alloy of 90% Cu and 10% Ni alloy are shown in fig. 2. For copper λ is increasing with decreasing temperature until a maximum is reached near 20K. This increase is typical for pure metals [6]. In alloys due to phonon scatter-

ing at the foreign atoms and lattice imperfections this increase is only weakly existent or rather completely missing [6]. Tempered probes exhibit a higher conductivity which can be explained by healing of lattice defects.

The thermal conductivity of the CuCrZr-alloy used for L42-combustor has been determined experimentally in the range 4K-293K (fig. 3). The decrease of λ at low temperatures typical for alloys has been observed. For numerical simulations the temperature dependence λ(T) of our material has been approximated by the red line shown in fig. 3.

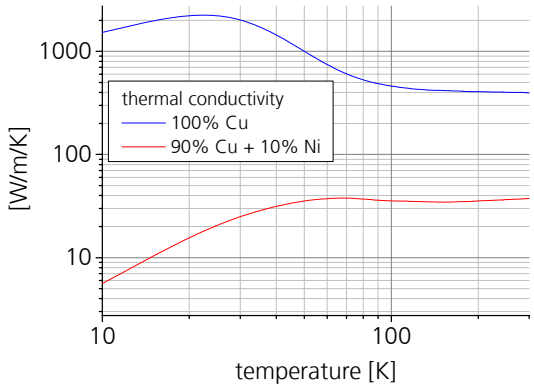

Fig. 2

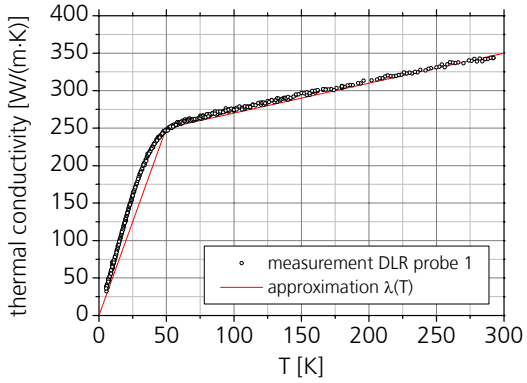

Fig. 3

Thermal Expansion Coefficeint

The anharmonicity of the interaction potential between lattice atoms results in thermal expansion of the solid. For a harmonic potential

(1) $$U(x) = cx^2$$

the oscillation of the atoms around their equilibrium position would be symmetric for all temperatures. The mean distance between lattice atoms would be constant, no thermal expansion would be observed. For a better approximation the potential is developed in a Taylor-series around its minimum at the equilibrium distance x_e:

(2) $$U(x) = cx^2 - gx^3 + \ldots$$

The term gx^3 is responsible for the asymmetry of the potential and for the mean distance between two lattice atoms one gets [5]

(3) $$\langle x \rangle = x_e + \frac{3g}{4c^2} k_B T$$

The thermal expansion coefficient can be derived from the mean distance <x>:

(4) $$\alpha = \frac{1}{\langle x \rangle} \frac{d\langle x \rangle}{dT} \cong \frac{3}{4} \frac{g k_B}{x_e c^2}$$

This simple approximation predicts a constant expansion coefficient α. At low temperatures experiments show a temperature dependence of α. The thermal expansion and the corresponding expansion coefficient for Cu are plotted in fig. 4. α(T) approaches zero at low temperatures and is rather constant for T>150K. The expansion coefficient is not sensitive to impurities in the solid, thus the data are a good approximation for the properties of our alloy.

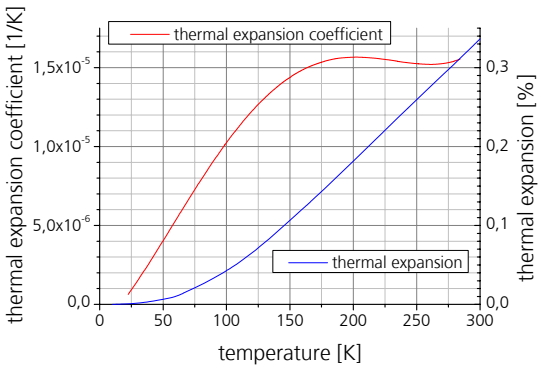

Fig. 4

Combustion Chamber L42 for Heat Transfer Investigations in Cooling Channels

For basic investigations of technologies for regenerative cooling the modular combustor L42 has been developed at DLR Lampoldshausen, which allows testing combustion chamber modules of various functionalities. One segment is especially dedicated to investigate heat transfer in cooling channels with high aspect ratio. This HARCC-segment (HARCC: High Aspect Ratio Cooling Channel) has around its circumference four 90° sectors each with cooling channels of a different aspect ratio ranging from 1.7 to 30 (Table 1). In the hot runs the structural temperature is measured at several axial positions. At these positions the temperature is determined at various distances from the hot gas wall with thermocouples (Fig. 5). Details concerning the design and manufacturing of the HARCC segment can be found in [3]. In the following the temperature field is discussed at two axial positions, position 1, 52.5mm and position 2, 152.5mm downstream stream the cooling fluid inlet.

With inverse methods from the temperatures measured at discrete locations the thermal field in the wall structure is reconstructed [7]. In this context the question arose, how the temperature dependence of the thermal conductivity influences the resulting solution for the thermal field.

The combustor wall is manufactured from different materials (Fig. 6). The hot gas wall is build from the CuCrZr-alloy. The cooling channels are closed with a layer of galvanic deposited copper (eCu), a galvanic Ni-layer (eNi) is added to withstand the mechanical loads. The values for the thermal conductivity used in the analysis are summarized in Table 2. The value for the CuCrZr-alloy is from the material data sheet and has been determined at room temperature.

To identify the influence of the temperature dependence of the thermal conductivity the thermal fields are determined first assuming constant λ using the value of Table 2 for the CuCrZr-alloy. Then the thermal field is calculated assuming the temperature dependence $\lambda(T)$ as plotted in Fig. 4. The thermal conductivities for eNi and eCu has been kept constant in both cases. The operational points chosen in the following correspond to test cases experimentally investigated at the HARCC-segment [7].

Table 1

sector	width [mm]	height [mm]	AR H/B
Q1	1.2	2	1.67
Q2	0.8	2.8	3.5
Q3	0.3	9.0	30.0
Q4	0.5	4.6	9.2

Table 2

	eNi	eCu	CuCrZr
[W/m/K]	75	400	350

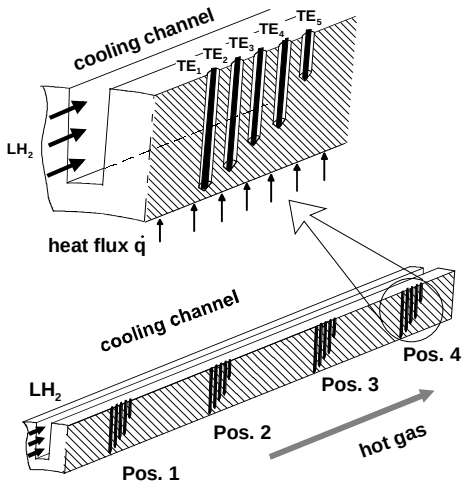

Fig. 5

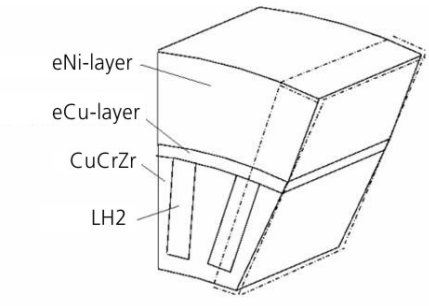

Fig. 6

Temperature Field at Stationary Conditions

The wall temperature is calculated using the commercial code FlexPDE. For a 2D-geometry representing the cooling channel cross sections and the materials of the wall the heat conduction equation is solved numerically:

(5) $$\nabla \cdot (\lambda \nabla T) = 0$$

On the hot gas- and coolant-sides following boundary conditions have been assumed:

(6) $$\frac{\partial T}{\partial n} = \alpha_{HG}(T_{HG} - T)$$

on the hot gas-side and

(7) $$\frac{\partial T}{\partial n} = \alpha_{CF}(T_{CF} - T)$$

on the cooling channel side.

The hot gas temperature T_{HG} and the temperature of the cooling fluid T_{CF} as well as the heat transfer coefficients on the hot gas side α_{HG} and the coolant side α_{CF} have been chosen corresponding to the results of the analysis of the experimental data from the HARCC-segment. α_{CF} is assumed to be constant along the circumference of the cooling channel. The boundary conditions for the determination of the thermal fields at axial positions 1 and 2 are summarized in Tables 3 and 4. The main difference is due to the temperature increase of the coolant at the downstream position 2 as compared to the upstream position 1.

In fig. 7 the computational area and the thermal conductivity of the different materials is shown for a temperature dependent λ(T) of the CuCrZr-alloy. Clearly the reduction of λ(T) in low temperature regions in the CuCrZr-layer is seen.

For axial position 1 the difference $\Delta T_W = T_v - T_c$ between the thermal fields T_c obtained assuming constant λ and T_v assuming a temperature dependent thermal conductivity λ(T) is shown in Fig. 8 for aspect ratios of H/B=1.7 and H/B=30. The low value of λ in the cold regions results in an increase of temperatures near the hot-gas side and a decrease in the other regions. With increasing aspect ratio the heat flux through the cold fins increases as compared to the flux through the bottom of the cooling channel. Due to the cold temperatures in the fins λ(T) decreases there and higher hot gas-wall temperatures result as compared to the case with constant λ. In table 5 the differences ΔT_W of the hot gas-side wall temperatures are listed for the four aspect ratios. Assuming a temperature dependent λ(T) for H/B=30 the hot-gas wall temperature is 9.1K above the value obtained with constant λ.

The temperature in the wall structure increases downstream due to the increase of the temperature of the cooling fluid. The reduction of λ(T) in the cold regions is less significant. As can be seen in table 6 at the downstream position 2 ΔT_W is reduced.

For the simulations up to now cooling fluid temperatures have been chosen resulting from the analysis of stationary flow conditions at the HARCC experiments. However in combustion chambers the temperature of LH2 at the cooling channel inlet can be significantly colder. Therefore the analysis has been done for an assumed temperature T_{H2}=50K for cooling fluid. The heat transfer coefficients have been chosen according to table 3.

The colder cooling fluid reduces the wall temperature and therefore the temperature dependent λ(T). As can be seen in fig. 9 and table 7 the hot gas-side wall temperature is increased by up to 29.7K in the case of temperature dependent λ(T).

Table 3

position 1		T_{HG}	α_{HG}	T_{H2}	α_{CF}
H/B	sector	[K]	[W/m^2/K]	[K]	[W/m^2/K]
1.7	Q1	3347	1.03e4	85	1.00e5
3.5	Q2	3347	1.03e4	90	1.04e5
9.1	Q4	3347	1.03e4	95	1.08e5
30	Q3	3347	1.03e4	100	1.13e5

Table 4

position 2		T_{HG}	α_{HG}	T_{H2}	α_{CF}
H/B	sector	[K]	[W/m^2/K]	[K]	[W/m^2/K]
1.7	Q1	3347	1.03e4	125	1.3e5
3.5	Q2	3347	1.03e4	137	1.3e5
9.1	Q4	3347	1.03e4	149	1.3e5
30	Q3	3347	1.03e4	160	1.3e5

Table 5

position 1		T_W [K]		ΔT_W [K]
H/B	sector	λ=const.	λ(T)	
1.7	Q1	380.9	385.0	4.9
3.5	Q2	363.3	369.4	6.1
9.1	Q4	349.9	358.2	8.3
30	Q3	343.6	352.7	9.1

Table 6

position 2		T_W [K]		ΔT_W [K]
H/B	sector	λ=const.	λ(T)	
1.7	Q1	386.2	391.2	4.0
3.5	Q2	385.1	390.9	5.8
9.1	Q4	385.7	392.1	6.4
30	Q3	389.5	395.4	5.9

Table 7

position 1		T_W [K]		ΔT_W [K]
H/B	sector	λ=const.	λ(T)	
1.7	Q1	349.0	361.3	12.3
3.5	Q2	326.6	345.7	19.1
9.1	Q4	308.3	334.6	26.3
30	Q3	297.3	327.0	29.7

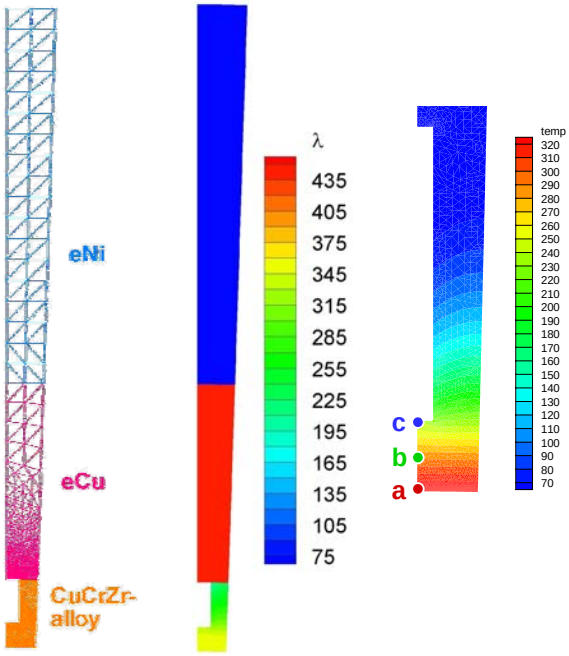

Fig. 7

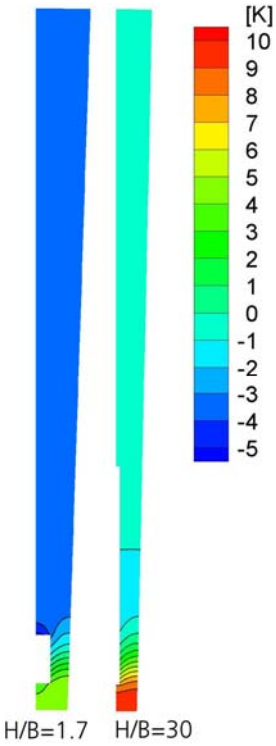

Fig. 8

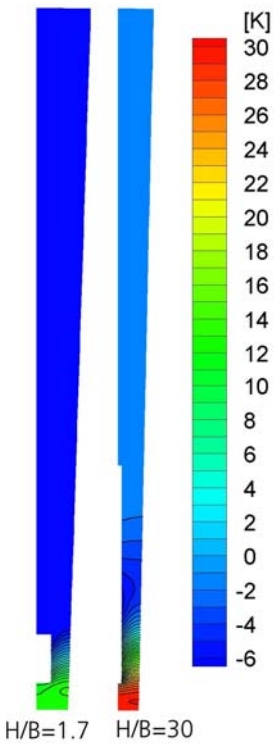

Fig. 9

Transient Temperature Fields

The instationary heat transfer problem is analysed based on following differential equation:

$$\rho c_V(T)\frac{\partial T}{\partial t} - \nabla\cdot(\lambda\nabla T) = \dot{W} \quad (8)$$

There are no heat sinks or sources in the structure, therefore there is $\dot{W} = 0$. On the hot gas- and coolant-side according to boundary conditions (6) and (7) it is

$$\dot{W} = -\alpha_{HG}(T_{HG} - T) \quad (9)$$

on the hot gas-side and

$$\dot{W} = -\alpha_{CF}(T_{CF} - T) \quad (10)$$

on the coolant side.

At LH2-temperatures c_V decreases to a view percent of its value at ambient temperatures. Looking to equation (8) one could expect high temporal gradients at these conditions. To evaluate the consequences of c_V (T) the transient evolution of the thermal field in the structure is analysed when the hot gas wall temperature T_{HG} is instantaneously increased from 40K to 3347K. The results assuming a constant value of the specific heat of c_0=385 J/kg/K are compared with that of a temperature dependent value $c_V(T)$ as shown in fig. 1.

The temperature of the coolant was 40K in this simulation, the hot gas- and coolant-side heat transfer coefficients were $\alpha_{HG}=1.033\cdot10^4$ W/m^2/K and $\alpha_{CF}=1.083\cdot10^5$ W/m^2/K. The thermal conductivity was modelled according the temperature dependence shown in fig.3. The evolution of the thermal field is evaluated at three positions in the wall (see fig. 7). The instantaneous temperature increase is switched on at t=0.

The assumption of a temperature dependent specific heat results at all three position in a faster increase of temperature, the thermal wave enters the combustor wall more quickly. As shown in fig. 10 at a specific time the maximal difference in temperatures as compared to the assumption of constant c_0 is always below 30K. In both cases the highest temperatures are reached at stationary conditions after about 100ms.

The temporal temperature gradients are as expected higher when assuming a temperature dependent $c_V(T)$ as compared to constant c_0 (see fig. 11). On the hot gas-wall after 0.1ms the difference is about a factor of 1.7, the difference is disappearing when approaching stationary conditions. At all evaluated positions after 10ms the rate of temperature variation is rather identical.

At t=0 the highest spatial temperature gradients are observed at position *a* on the hot gas side (fig. 12). At this position a temperature dependent specific heat $c_V(T)$ results in a gradient somewhat below that assuming constant c_0. Inside the combustor wall and at the bottom of the cooling channel the gradients start to increase later. For positions b and c with assumption of a temperature dependent $c_V(T)$ one gets larger gradients than with constant c_0. The differences in the spatial gradients are however not very pronounced.

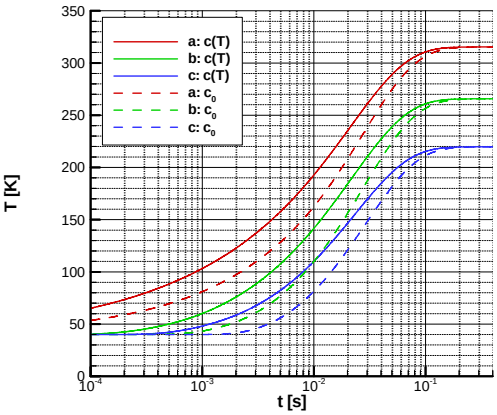

Fig. 10

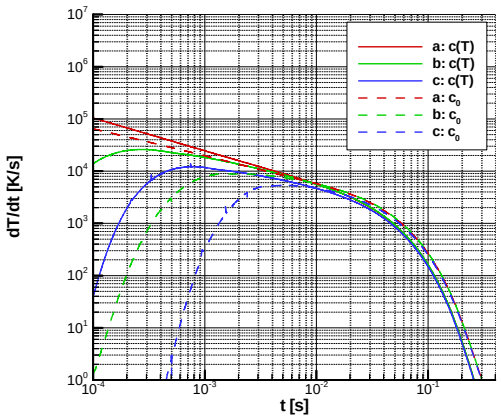

Fig. 11

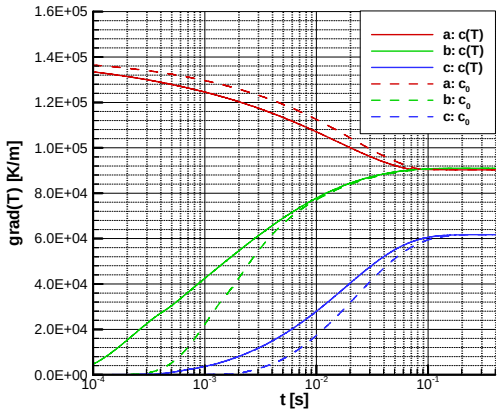

Fig. 12

Summary and Discussion

In the temperaure range typical for wall structures of cryogenic combustors the thermal conductivity, the specific heat, and the thermal expansion coefficient vary significantly for Cu-alloys. The values of all three properties approach zero at very low temperatures.

The decrease of the thermal conductivity results in an increase of the hot gas-wall temperature. This increase can be significant especially near the cooling fluid inlet, when its temperature is still low and λ is reduced strongly.

The decrease of the specific heat results in a faster penetration of the thermal wave into the structure when the hot gas temperature is increased instantaneously. However in view of the pronounced variation of c_V with temperature the thermal transients show only minor differences as compared to assuming a constant specific heat.

References

1. J. Riccius, E.B. Zametaev, Stationary and dynamic thermal analysis of cryogenic liquid rocket combustion chamber walls, AIAA 2002-3694, 38th Joint Propulsion Conference, 2002
2. Fröhlich, M. Popp, G. Schmidt, D. Thelemann. Heat Transfer Chraracteristics of H2/O2 Combustion Chambers, AIAA 93-1826, 29th Joint Propulsion Conference, Monterey, CA, 1993
3. D. Suslov, A. Woschnak, J. Sender, M. Oschwald, Test specimen design and measurement technique for investigation of heat transfer processes in cooling channels of rocket engines under real thermal conditions, AIAA 2003-4613, 39th Joint Propulsion Conference, Huntsville, 2003
4. C. Kittel, Introduction to Solid State Physics, John Wiley and Sons, 1986
5. N.W. Ashcroft, N.D. Mermin, Solid State Physics, CBS Publishing Asia Ltd., 1987
6. R.L. Powell and W. A. Blanpied, Thermal Conductivity of Metals and Alloys at Low Temperature, NBS Circular 556, 1954
7. Woschnak, D. Suslov, M. Oschwald, Experimental and Numerical Investigations of Thermal Stratification Effects, AIAA 2003-4615, 39th Joint Propulsion Conference. Huntsville, 2003